Effect of Electric Potential on the Structure and Yield of Graphene Oxide using Electrochemical Exfoliation Method

O. D. Adigun[1, 2, *], L. E. Umoru[2], T. N. Iwatan[1]

[1] Department of Materials and Metallurgical Engineering, Federal University Oye Ekiti, Nigeria
[2] Department of Materials Science and Engineering, Obafemi Awolowo University, Ile-Ife, Nigeria

ABSTRACT: Optimization of the electrochemical exfoliation of graphene oxide synthesis was investigated in this report using varying potentials. Graphite from waste lithium-ion batteries was used as the electrodes for the DC (direct current) electrochemical set-up. Electric potentials of 7.5 V, 12 V, and 15 V were applied for 225 minutes using 0.2M H_2SO_4 as the electrolyte. The characterization of the produced graphene oxide was done using Raman spectroscopy, high-resolution scanning electron microscopy (HRSEM), and energy dispersive x-ray spectroscopy (EDS) attached to the scanning electron microscope (SEM). The results obtained showed that both the rate of graphene oxide yield and the C/O ratio increased correspondingly with the increase in electric potential. However, the structure of graphene oxide produced at 7.5 V was of superior quality compared to others produced at higher potentials with regards to the crystallite lattice characteristics such as defects, lateral dimensions, thickness, and the number of graphene layers. Consequently, tailor-made graphene oxide properties (and yield) for target applications may be achieved using the electrochemical exfoliation method via the choice of the electric potential.

KEYWORDS: Graphene oxide, Electrochemical exfoliation, Electric potential/voltage, Yield, Quality

[Received Dec. 21, 2022; Revised Mar 27, 2023; Accepted April 14, 2023] Print ISSN: 0189-9546 | Online ISSN: 2437-2110

I. INTRODUCTION

Graphene is a two-dimensional single atom of carbon arranged in a honeycomb crystal (Liu *et al*., 2019). Over the years, the fascinating electrical (Shen *et al*., 2017; Yue *et al*., 2019), thermal (Li *et al*., 2016), optical (Baker and Baker, 2010; Yoo *et al*., 2019), and mechanical (Wang *et al*., 2019) properties of graphene have been demonstrated in applications where exceptional electronic, high temperature stability, radiation shielding, energy conversion and storage, and structural stability are of valuable importance (Liu *et al*., 2019). But despite the promising possibilities for cutting-edge improvements in the performance of graphene-boosted properties in allied materials, some challenges surrounding the synthesis of high-quality graphene and the difficulty in devising a cost-effective mass production approach are barriers to the commercial exploitation of the material. Graphene can be produced by different methods. Common among the methods are chemical vapour deposition (CVD) (Frank and Kalbac, 2014), electrochemical exfoliation of graphite (Liu *et al*., 2019), epitaxial growth on an electrically insulating surface (Liu *et al*., 2020; Sinterhauf *et al*., 2021), solvothermal synthesis (Lellala, Namratha and Byrappa, 2016), and the reduction of graphene oxide (GO) (Hou *et al*., 2018). Among these, the electrochemical exfoliation approach has attracted definite attention due to its relatively cheap, manageable, and eco-friendly processes with mass production capabilities. Basically, electrochemical exfoliation of graphite is achieved when an applied voltage (potential) promotes ionic components within the electrolyte to penetrate and intercalate the graphite, where they produce gaseous species that cause flaking off of the thin graphene oxide sheets by the exfoliation of the single graphite layers. The synthesis typically utilizes the application of electricity to enhance the structural expansion (via cathodic reduction and/or anodic oxidation) of a graphite working electrode (that is normally in the form of a rod, flake, or HOPG-highly oriented pyrolytic graphite) in a liquid electrolyte (aqueous: acidic, surfactant, or non-aqueous) to inspire the shedding off of the graphene oxide layers. The electrochemical exfoliation reaction experiments are mostly done in ionic liquids or acidic aqueous electrolytes (Achee *et al*., 2018). In a typical electrochemical synthesis of graphene, two electrodes will be used as the cathode and anode. Graphite can be used as both electrodes, but a number of studies have been carried out using graphite as the anode and a metal (e.g., platinum) as the cathode for the electrochemical exfoliation process (Li *et al*., 2020). The primary indicators that control the intercalation and electrochemical exfoliation of the graphene flakes include the electrolyte type, the electrolyte concentration, and the voltage (Yoon *et al*., 2015; Achee *et al*., 2018). So far, studies concerning these indicators are still very rare in the literature, and there is less emphasis on the influence of potential on the structure and yield of the synthesized graphene oxide (Htwe *et al*., 2019; Liu *et al*., 2019; Ilias, Murshidi and Ying, 2021). Till date, there appears to be no

*Corresponding author: oluwole.adigun@fuoye.edu.ng
doi: http://dx.doi.org/10.4314/njtd.v18i4.1521

comprehensive published report that presents the effect of electric potential on the structure and yield of graphene; capturing information about the C/O ratio, production rate, and crystallite parameters using the electrochemical exfoliation method; any contribution to knowledge in this regard could further enhance the understanding on the efficiency or optimization of the electrochemical exfoliation technique; and this is where the current study comes in.

Graphene and graphene oxide are both forms of graphene. While graphene is pure and possesses the pristine properties of the in-situ material, graphene oxide is a form of graphene that has been chemically modified (or contaminated) with oxygen-containing functional groups, such as hydroxyl and carboxyl groups. This modification makes graphene oxide easier to process and manipulate, but it also reduces its electrical and mechanical properties (Razaq *et al.*, 2022). Despite its reduced properties, graphene oxide still has many potential applications, such as in water filtration, energy storage, and biomedical engineering (Ajala *et al*., 2022). Moreover, depending on the specific application and the desired properties of the final graphene material, graphene oxide may be converted to reduced graphene oxide using several methods that can reduce the oxygen-containing functional groups in graphene oxide. Some of these reduction methods can be achieved using chemical agents (Kurian, 2021), thermal treatments (Acik *et al*., 2011), electrochemical reduction (Toh *et al*., 2014), laser-induced reduction (Tran *et al*., 2018), and microwave-assisted reduction (Xie, Zhou and Huang, 2019). In the present study, however, the graphene oxide synthesized from the selected electric potentials is not reduced since our focus is on investigating how the choice of electric potential may influence the yield, C/O ratio, and structure of the resulting graphene material with a view to appraising the processes leading to the observed results.

Considering the vital role batteries play in the zero-emission framework (as applicable to electric cars) and energy storage, their production, sustainability, and usage are now of important interest in emerging economies across the world. The widespread ecological impacts of evolving contaminants from battery waste and the ensuing medical and economic concerns were recently revealed by references (Melchor-Martínez *et al*., 2021; Rey *et al*., 2021), with emphasis on the carbon-based and ionic liquid contaminants besides the heavy metal toxins. The carbon-based contaminants basically emanate from the graphite component of the battery waste, and efforts at recycling the graphite waste have been attempted in a few studies (Gao *et al*., 2020; Liu *et al*., 2022). Besides the suggested regeneration approaches, recent developments have proposed the use of graphite from waste sources as an electrode material for graphene synthesis (Singh, 2021). This invariably presents an alternative measure to convert the waste material into useful substitutes for other scientific applications. We propose that the high associated cost of graphene production may be partly mitigated by the use of graphite from waste batteries. Consequently, the effect of different voltage biases on the yield and properties of graphene produced using the electrochemical exfoliation method, utilizing graphite electrodes from waste lithium-ion batteries, has been presented in the current study, with valuable information divulged.

Graphene oxide can be characterized using techniques such as atomic force microscopy (AFM), transmission electron microscopy (TEM), x-ray photoelectron spectroscopy (XPS), scanning electron microscopy (SEM), Fourier transform infrared spectroscopy (FTIR), energy dispersive x-ray spectroscopy (EDS), Raman spectroscopy, and x-ray diffraction (XRD). AFM provides 3D images that help investigate the lateral dimensions, thickness, and number of layers of graphene film (Shearer *et al.*, 2016). SEM can be deployed to assess the morphology of the material. Both structural quality and numbers of layers can be determined using TEM (Mbayachi *et al*., 2021). FTIR and XPS help to study structural integrity by revealing information about the residual functional groups and the presence of foreign atoms, respectively (Hu, Yao and Wang, 2017). XRD basically identifies the phases based on the units of dimension (Mbayachi *et al.*, 2021), while Raman spectroscopy is generally a versatile technique to quantify and identify defects, evaluate the structure, and assess the lateral dimensions, thickness, and number of graphene layers in graphitic materials (Wall, 2011; Cançado *et al*., 2017; Lee *et al*., 2017). It is worth mentioning that the Raman spectroscopy characterization tool is swift, non-destructive, and can give structural information with very high resolution, and the data generated can be extrapolated to provide a wide range of details beyond the capacity of the other techniques. Such details may include perturbation effects like doping, disorder, strain, magnetic and electric fields (Ferrari and Basko, 2013). Moreover, the three main Raman modes that reveal the presence of graphene, i.e., the G, D, and 2D bands, provide a lot of information about the quality of the material, especially when the intensity and shape profile are quantified. The quality of graphene can be judged by the defect level, size of the lateral dimension, sheet thickness, and graphene oxide sheets (Cançado *et al*., 2017). Smaller lateral size corresponds to lower crystallinity, and a smaller lateral size corresponding to lower crystallinity would invariably result in low quality graphene oxide (Wu *et al*., 2009). In its finest state, graphene exists as a monolayer material, but stacking the layers into a multilayer may also retard its properties. Defects distort the usual hexagonal honeycomb structure of graphene, which leads to imperfection and deviation in the arrangements of the atoms, bond length, and edge orientations that, in turn, alter the properties. Defects can be generated during crystal growth, particle irradiation, and reaction of carbon atoms with other species during synthesis (Liu *et al*., 2015). The fact that defects in graphene oxide are generated during synthesis makes them difficult to prevent. However, understanding the mechanisms that may lead to the defects would be useful in devising measures to synthesize high-quality graphene for useful applications.

In this study, the process efficiency and structure of graphene oxide produced by different potentials (7 V, 12 V, and 15 V) using electrochemical exfoliation techniques were investigated while maintaining a uniform electrolyte type, exfoliation time, dimension and type of electrode, volume of the electrode immersed in the electrolyte, ultrasonic sonication time, electrolyte concentration, and all other experimental conditions. The investigation is supported with high-resolution scanning electron microscopy (HR-SEM), Raman

spectroscopy, and energy dispersive x-ray spectroscopy (EDS) through a novel characterization protocol with established models to assess the influence of the potentials on graphene yield and the structure of graphene oxide produced. Differences among the structure and disorder of the synthesized graphene oxide using the various potentials were examined, giving due attention to the mechanisms and chemistry behind the observed changes. The defect concentration and overall structure of the synthesized graphene oxide are examined with a view to identifying the finest voltage selection that could most suitably fit graphene mass production using the electrochemical exfoliation approach. The reported effects of the selected electric potentials on a combination of the C/O ratio, structure, and yield of the synthesized graphene materials as well as the novel structure characterization approach employed make the current study unique. The information in this report could further enhance understanding of the optimization of the electrochemical exfoliation technique over the electric potential for the synthesis of graphene with tailor-made improved quality, quantity, and properties.

II. EXPERIMENTAL PROCEDURE

The anode and cathode of the electrochemical set-up consist of locally sourced graphite rods from waste lithium-ion batteries that were thoroughly washed using distilled water. The initial dimensions and weight of the graphite rods were taken, and voltages of 7.5 V, 12 V and 15 V were applied for 225 minutes each in 0.2 M H_2SO_4 electrolyte connected to a DC power supply via jumper cables for the electrochemical process. In this process, the concentration of the electrolyte, the volume of graphite electrode immersed in the electrolyte, and the electrolyte used are kept constant; only the potential is varied. The electrolyte solution is found to change from a colourless to a dark colour with time as intercalation and exfoliation occur; and the mass of each electrode is recorded at intervals in order to monitor the weight loss with respect to time. Afterwards, the flake-electrolyte mixture is collected into 20 ml tubes for separation in a centrifuge machine (Model 800D: 6 x 20 ml holes) before washing with distilled water and acetone. Subsequently, the graphene oxide powder is placed in sample bottles containing a solution of distilled water mixed with acetone in the ratio 4:1 and sonicated for 120 minutes in an ultrasonic bath holding deionized water (Sororex Super RK 514 BH, Bandelin). The sonicated mixture is then dried using hot air in a laboratory oven at 100 ^oC for 120 minutes. The produced graphene oxide was characterized using Raman spectroscopy (HR Raman Spectroscope HR800, Horiba Jobin Yvon GmbH), scanning electron microscope, SEM (Philips XL30 FEG, USA), and energy dispersive x-ray spectroscopy (EDS) attached to the SEM equipment. Further information about the experimental approach is presented in Figure 1.

III. RESULTS AND DISCUSSION

A. Assessment of the nanocarbon structure

The structures of the anodic electrochemically exfoliated graphene oxide produced using 7.5 V, 12 V, and 15 V were examined by Raman spectroscopy. In all tested samples, as illustrated in Figure 2, the famous first order G and D bands common to graphene-based materials were observed between approximately 1350 and 1590 cm^{-1}, while the bands associated with the second order Raman spectra (i.e., 2D or G' and D + G bands) could be seen around 2350 – 3350 cm^{-1}. The G band corresponds to the two dimensional Raman vibration of the sp^2 in-plane carbon atoms motion with the E_{2g} optical phonon symmetry that provided information on the honeycomb lattice structure of the nano-carbon phase, while the D band is due to scattering from ring breathing modes of the disordered sp^2 carbon atoms (with A_{1g} symmetry) that gives information about the local defects, edge structure, and dangling sp^2 carbon bonds present in the graphene oxide structure (Munuera *et al.*, 2016, 2017; Shinde *et al.*, 2016). The 2D (or G') band is an overtone (second order spectrum) of the D band, showing the stretching vibration of the proton promulgated by double resonance close to the corners of the Brillouin zone, and provides details about the electronic structure as well as the stacking order (or layer) of the graphene oxide (Jorio *et al.*, 2011).

All the collected Raman spectra from the samples prepared using the 7.5 V, 12 V, and 15 V voltages showed the three prominent Raman peaks, comprising the G band at ~1584 cm^{-1}, the D band at ~1356 cm^{-1} and the 2D band at ~2703 cm^{-1} (see Figure 2). In monolayer graphene, the 2D (G') band is often a single peak. Splitting of the 2D (G') band into 2D (G'), D + D' and 2D' (or G") by the tested potentials revealed some degrees of structural disorder and the presence of a few-layers of graphene oxide. This is a known feature in the Raman scatter of the sp^2 carbon phase in graphene or graphene oxide (Cançado *et al.*, 2011; Jorio *et al.*, 2011; Wall, 2011).

For any given lesser wavelength (λ_L), the reported disorder-induced D band intensity (I_D) of a graphitic Raman spectrum can be measurably related to the ordered G band intensity (I_G) to give information about the (in-plane) crystallite size (L_a). In agreement with the correlation between L_a and the integrated area ratio I_D:I_G in recent studies (Matthews *et al.*, 1999; Cançado *et al.*, 2006; Ferrari, 2007), the structure of the synthesized graphene oxide series was examined by the magnitude of the lateral crystal size (L_a), defect density (η_D), inter-defect distance (L_D), and average continuous graphene length including tortuosity (L_{eq}) using Eqns (1 to 4) (Pimenta *et al.*, 2007; Larouche and Stansfield, 2010; Rothermel *et al.*, 2016; Wu *et al.*, 2018) as presented in Table 1. Where λ_L is the laser wavelength (514.5 nm); I_D, I_G, and I_{2D} are the integrated intensities of the D, G, and 2D bands. Meanwhile, complementary information were deduced from the shape profiles of the first- and second-order spectra at < ~1600 cm^{-1} and between 2200-3500 cm^{-1}, respectively.

$$L_a = (2.4 \times 10^{-10})\, \lambda_L^4 \left(\frac{I_D}{I_G}\right)^{-1} \quad (1)$$

$$L_{eq} = 33.6343 \left(\frac{I_{2D}}{I_D}\right) \quad (2)$$

$$L_D = \sqrt{(1.8 \times 10 - 9)\, \lambda_L^4 \left(\frac{I_G}{I_D}\right)} \quad (3)$$

$$\eta_D = \frac{2.4 \times 10^{22}}{\lambda_L^4} \left(\frac{I_D}{I_G}\right) \quad (4)$$

The lateral crystallite size, La, and the average continuous graphene length including tortuosity, L_{eq}, provide information

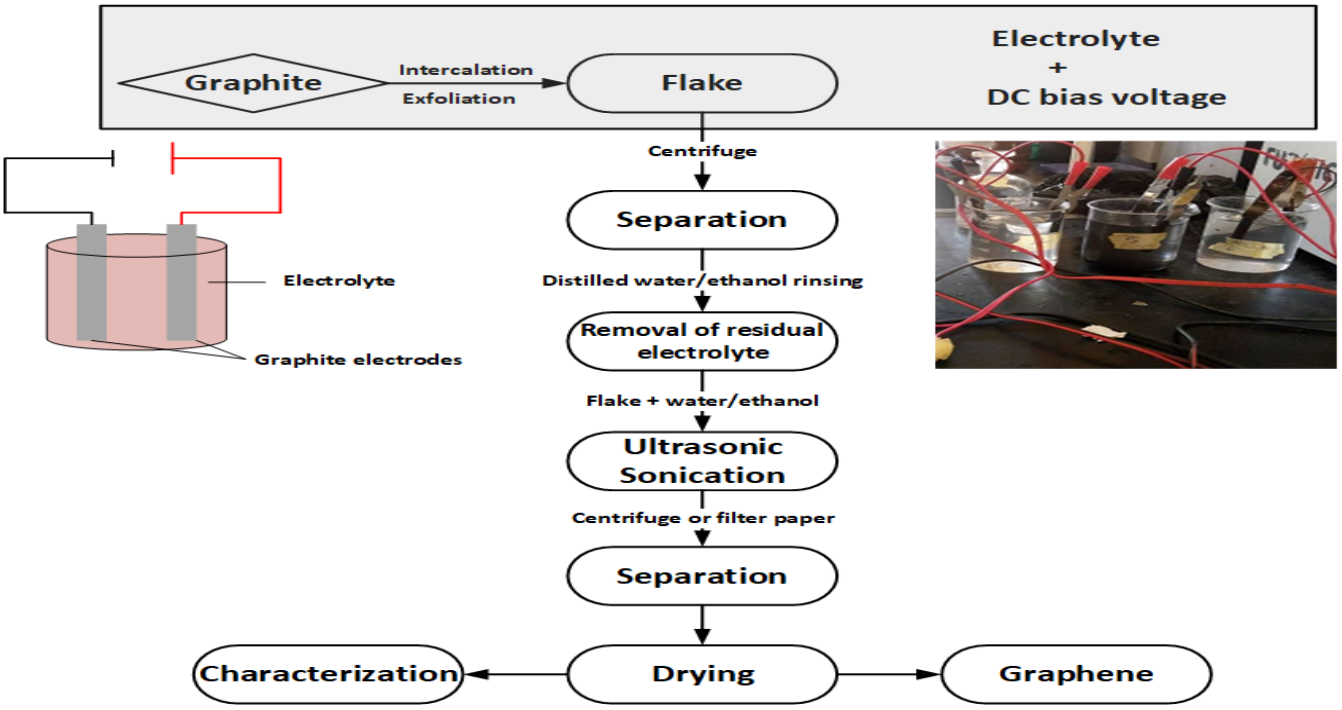

Figure 1: Schematic representation of the experimental process

on the crystal structure of graphene oxide. The lateral crystallite sizes of the graphene oxide synthesized using 7.5 V, 12 V, and 15 V were 22.93 nm, 15.93 nm and 12.11 nm, respectively. The lateral crystallite size was observed to decrease correspondingly with an increase in electric potential, indicating lower crystal growth in the graphene oxide synthesized at the higher potential. The lateral crystallite size corresponds to the crystallization of the sp^2 carbon phase, and a large crystallite size could enhance functional properties such as electrical properties and energy storage for reproducible high-capacity batteries (Pimenta *et al.*, 2007). The higher lateral crystal size of the graphene oxide produced by the 7.5 V potential could be attributed to the gentle flaking off of the thin graphene layers from the graphite electrode due to the comparably low voltage-prompted agitation of gaseous species within the electrolyte, leading to a mild or gentle intercalation and exfoliation energy required for transition towards crystal perfection. Clearly, the rate of production is favourably affected by the increase in potential, as revealed by the volume of graphene oxide produced from each potential setup. However, the high yield from the use of higher potential could be detrimental to the quality of graphene oxide and undesirable because the higher potential causes rapid intercalation and exfoliation of the graphene oxide and leads to mechanical faults that result in thick and abnormal flaws that reduce the crystallite size. Due to their unique properties and applications, the growth of LSSG (large-sized single-crystal graphene) or high-quality graphene with large crystallite sizes has been of interest to researchers over time, with the CVD approach being about the most widely discussed. However, controlling the epitaxial growth and nucleation of the graphene via i) reduction of the nucleation density, ii) prevention of multiple nucleation, and iii) enabling a seamless growth has presented some major challenges to the prevention of grain boundaries and defect concentration over the CVD method. On the other hand, the simplicity and suitability of the electrochemical exfoliation technique for mass graphene oxide synthesis could be enhanced for the production of larger graphene oxide crystallites by applying a considerably low potential to the electrodes for the intercalation and exfoliation processes.

The degree of graphitization of the synthesized graphene oxide materials is further corroborated by the determination of the average continuous graphene length including tortuosity, L_{eq}, using Equation (2) (Larouche and Stansfield, 2010). L_{eq} decreases with increasing potential, as shown in Table 1. The average continuous graphene length including tortuosity is an estimate of the equivalent phonon mean free path and reveals the presence of curvature, which is often present in graphene layers. Therefore, a finer crystal stability would be signified by an increase in the average continuous graphene length including tortuosity, L_{eq}. Inherently, the graphene oxide synthesized using 15 V shows the least L_{eq} value but the structural value, increases as the potential is reduced. Moreover, Larouch and Stansfield reported that L_{eq} permits better characterization of local dynamic properties than the lateral crystal size, La, and the presence of tortuosity (curvature) with well-connected graphene planar units is revealed when L_{eq} is greater than L_a ($L_{eq} > L_a$), as shown by the tested samples. In lieu of investigating imperfections in graphitic materials, the 2D band is practically dynamic at the curvature. Thus, the greater $\Delta\omega_{2D}^{-1}$ (FWHM of the 2D band) revealed in the graphene oxide planes synthesized using 7.5 V (see Figure 3) further corroborates the higher crystal quality/stability. Consequently, increases in L_{eq} with respect to the $\Delta\omega_{2D}^{-1}$, $\Delta\omega_{G}^{-1}$ and $\Delta\omega_{D}^{-1}$ indicate a higher graphitization quality (see Figure 3) (Larouche and Stansfield, 2010).

The number of graphene layers is estimated using I_G/I_{2D} and the results show that the structure contains 3 graphene layers (Table 1) (Björkman, 1969; Ferrari, 2007; Wall, 2011).

On the other hand, the graphene materials synthesized using 12 V and 15 V show shorter inter-defect distances (L_D) of 10.93 nm and 9.53 nm, respectively, than those synthesized using 7.5 V with an L_D value of 13.11 nm. Higher inter-defect distance values ordinarily lead to lower defect density within the graphene lattice. In essence, within the series of the examined potentials, 7.5 V reveals the highest L_D value that has the widest spread between neighboring defects within the structure of the produced graphene. As shown in Figure 2, the presence of the D band, which relates to structural disorder, confirms the existence of imperfections in the synthesized graphene oxide across the potentials. Note that pristine graphene does not show the Raman D peak (Pollard *et al.*, 2014).

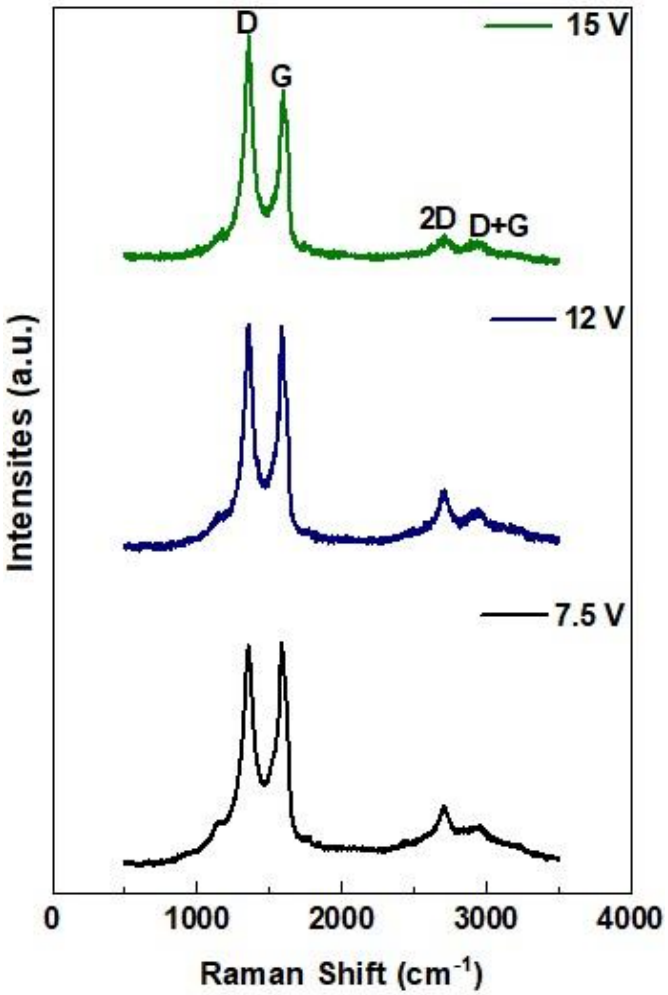

Figure 2: Raman spectra of graphene oxide synthesized using different electric potentials.

However, the distance between the defects and invariably the defect concentration is influenced by the selection of applicable potential during the synthesis. In essence, the larger inter-defect distance of 13.11 nm achieved at the lower potential of 7.5 V shows that selection of a comparably lower potential in the electrochemical exfoliation process could enhance high-quality graphene oxide synthesis via reduction in the lattice structural disorder, which is particularly achievable with a resultant high inter-defect distance (L_D) value and low defect concentration. The defect density, denoted as n_D is assessed using Eqn. (4). The defect density is observed to reduce with decreases in the applied potentials. The in-plane defects in graphene basically arise from both growth-induced flaws and natural imperfections, except for cases of artificially induced defects for the purpose of unique technological applications. The higher concentration of defects shown by the graphene synthesized at 15 V may be linked to the ensuing higher mechanical shearing during intercalation of the graphite. Moreover, as proposed by reference (Wu *et al.*, 2018), $\Delta\omega_G^{-1}$ basically increases with a decrease in defect density, as reported in Figure 3.

Table 1: Structure and disorder of the synthesized graphene oxide materials

Properties of graphene oxide	7.5 V	12 V	15 V
Number of graphene layer	3 layers	3 layers	3 layers
Average continuous graphene length including tortuosity, L_{eq} (nm)	21.49	10.39	5.54
Defect Distance, L_D (cm^{-2})	13.11	10.93	9.53
Defect density, x 10^{11} (nm)	2.51	3.61	4.76
Lateral crystallite size (nm)	22.93	15.93	12.11

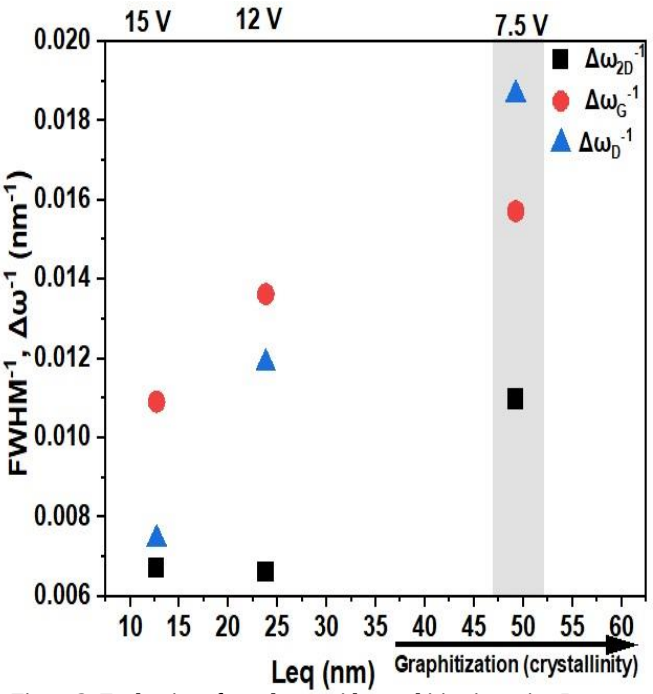

Figure 3: Evaluation of graphene oxide graphitization using L_{eq} as a function of $\Delta\omega_{2D}^{-1}$, $\Delta\omega_G^{-1}$ and $\Delta\omega_D^{-1}$

B. Morphology and elemental composition of the graphene oxides produced by the different electric potentials

The morphology of the synthesized graphene oxides was investigated using a high-resolution scanning electron microscope (HR-SEM). The SEM images of the graphene oxides typically show a flat, featureless surface, as the hexagonal lattice pattern is only visible at high magnifications. Depending on the sheet orientation, staking arrangements of agglomerated sheets can be seen in the SEM images. The images also reveal wrinkles, folds, and ripples in the graphene

structure (Figure 4). The tortuosity as described in Section 3.1 above is corroborated from the SEM images by the folding, irregular, and stretching layers of the graphene oxide sheets shown via the wrinkles and ripples.

The elemental composition of the graphene oxides synthesized by the different electric potentials was investigated using energy dispersive x-ray spectroscopy (EDS) attached to the scanning electron microscope (SEM).

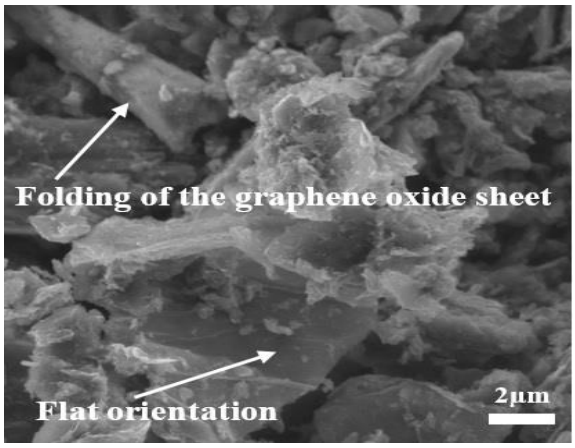

(ai)

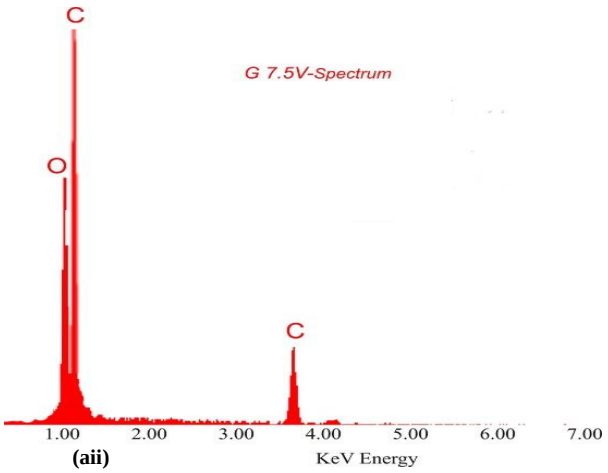

(aii)

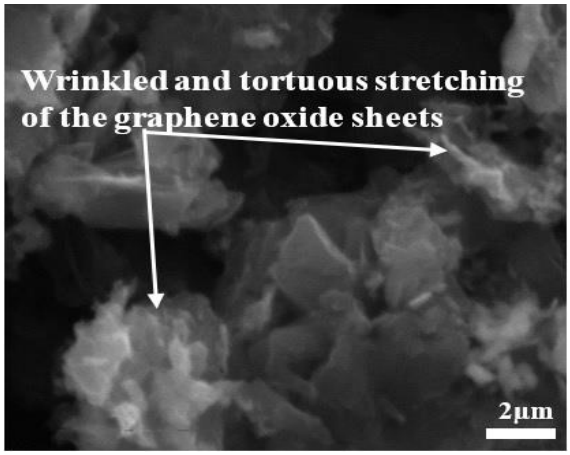

(bi)

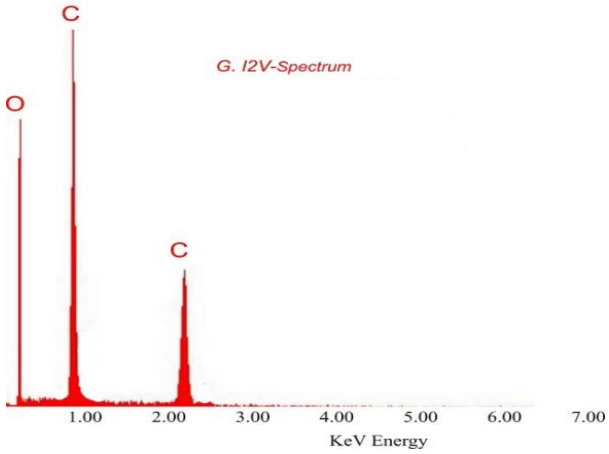

(bii)

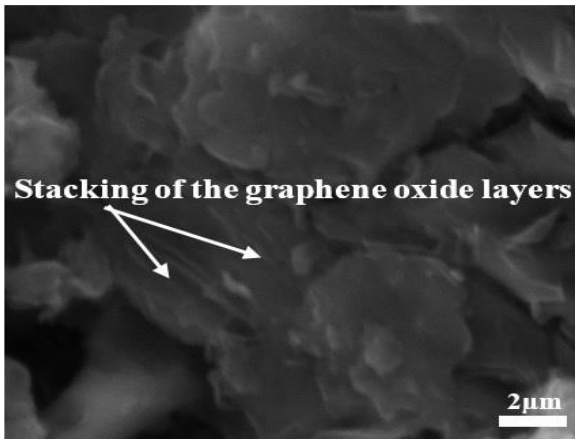

(ci)

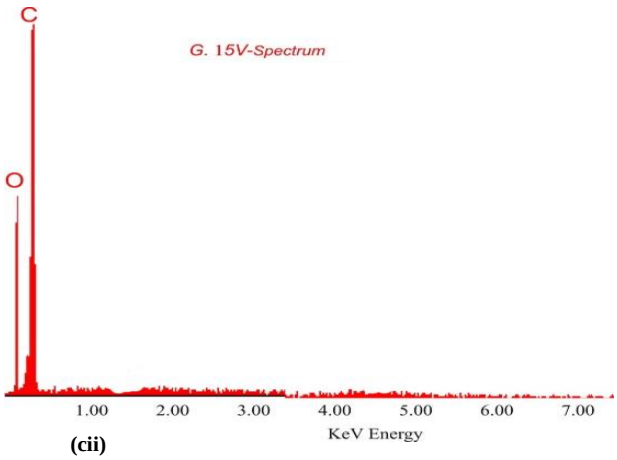

(cii)

Figure 4: SEM images and EDS spectra of the synthesized graphene oxides. a.i) Morphology of the graphene oxide synthesized using 7.5 V a.ii) EDS spectrum of the graphene oxide synthesized using 7.5 V b.i) Morphology of the graphene oxide synthesized using 12 V b.ii) EDS spectrum of the graphene oxide synthesized using 12 V c.i) Morphology of the graphene oxide synthesized using 15 V c.ii) EDS spectrum of the graphene oxide synthesized using 15 V

From the atomic compositions of carbon (C) and oxygen (O), it is observed that the C/O ratio increased correspondingly with the increase in electric potential (see Table 2). As shown in Section 3.3, the yield of graphene oxide appears to be proportional to the intensity of the electric potential within the investigated voltage range (i.e., from 7.5 V to 15 V); therefore, a combination of the high oxidation potential of the SO^{-}_{4} radical (+2.6 V) ion from the H_2SO_4 electrolyte, aided by the intensity of applied electric potentials, invariably intercalates the graphite layers to exfoliate the graphene sheets. However, as the intensity of the electric potential increases from 7.5 V to 15 V, the energy available to initiate the graphite interlayer exfoliation also increases, favouring the nanocarbon yield over the degree of oxidation by the SO^{-}_{4} radical and accounting for the observed increase in the C/O ratio as the intensity of the electric potential increases from 7.5 V to 15 V. As the choice of a lower electric potential had shown a finer graphene oxide structure and quality, as earlier discussed, the low C/O ratio shown by the lower electric potential may generally be increased using available reduction techniques, depending on the intended properties and application of the graphene material. Effectively, the choice of the most suitable potential for any graphene oxide production design (using the electrochemical exfoliation approach) may have to be carefully negotiated among the yield, C/O ratio, and quality.

Table 2: Chemical composition of the synthesized graphene oxide materials

Electric potentials	C/O ratio	Carbon content (at. %)
7.5 V	3.12	75.72
12 V	4.11	80.44
15 V	5.93	85.58

C. Yield of the graphene oxide produced by the different electric potentials

The rate of graphene oxide production over the applied potentials was investigated by measuring the mass of graphene oxide flaked from the graphite electrodes per hour for the duration of the electrochemical exfoliation process. For all the applied potentials, an average of 73% of the flaking occurred at the anode, while the cathode contributed 27% to the graphene oxide yield. The dilute H_2SO_4 electrolyte with 0.2 molarity was used across each applied potential, and the ions present in the electrolyte are SO_4^{2-}, OH^- (from water), and H^+ (from both water and acid). Both SO_4^{2-} and OH^- were attracted to the anode, while the H^+ migrated to the cathode electrode, but it is the OH^- that loses electrons to produce oxygen gas for the intercalation and exfoliation of graphite. Nevertheless, the high exfoliation efficiency role of SO_4^{2-} at the anode has been attributed to the possibility of reversible intercalation characteristics of the sulfate ion relative to the high repulsive binding energy between the graphene sheets (Lee *et al.*, 2020). Thus, the higher rate of flaking noticed at the anode could be attributed to the efficient intercalation role played by the SO_4^{2-} ion combined with the subsequent oxidation-enabled exfoliation of graphite into graphene oxide. Consequently, the highest rate of graphene oxide flake exfoliation from the applied potentials is shown at 15 V, followed by 12 V. In essence, the rate of graphene oxide yield increases correspondingly with an increase in the applied electric potential. However, a compromise between the graphene quantity and quality is essential for the selection of the most suitable design of experiment for a quality-quantity efficient production process enabled using the electrochemical exfoliation technique.

IV. CONCLUSION

In this study, the yield and structure of graphene oxide synthesized using the electrochemical exfoliation method with variable potential (7.5 V, 12 V, and 15 V) were successfully determined. The structure of the synthesized graphene oxide examined using Raman spectroscopy, high-resolution scanning electron microscopy (HR-SEM), and energy dispersive x-ray spectroscopy (EDS) attached to the scanning electron microscope (SEM) revealed that the quality of the produced graphene oxide increased correspondingly with a decrease in the applied potential. Hence, the graphene oxide synthesized using 7.5 V showed the lowest defect concentration and the finest crystalline quality. On the other hand, the rate of graphene oxide yield investigated by the exfoliated mass at the electrodes over experiment duration is found to increase progressively with an increase in the applied electric potentials. The C/O ratio also shows a proportional increase with the increase in the potential from 7.5 V to 15 V. Consequently, a compromise among the yield, C/O ratio, and structure of the produced graphene oxide must be considered in the design of processes for mass production using the electrochemical exfoliation technique with respect to the electric potential applied.

AUTHOR CONTRIBUTIONS

O. D. Adigun; Conceptualization, Formal analysis, Investigation, Methodology, Resources, Writing – review & editing, **T. N. Iwatan;** Methodology, Supervision, **L. E. Umoru;** Writing – original draft, All authors have read and agreed to the published version of the manuscript.

REFERENCES

Achee, T. C.; W. Sun; J. T. Hope; S. G. Quitzau; C. B. Sweeney; S. A. Shah; T. Habib and M. J. Green. (2018). High-yield scalable graphene nanosheet production from compressed graphite using electrochemical exfoliation. *Scientific Reports*, *8*(1), 1–8. https://doi.org/10.1038/s41598-018-32741-3.

Acik, M.; G. Lee; C. Mattevi; A. Pirkle; R. Wallace; M. Chhowalla; K. Cho and Y. Chabal. (2011). The role of oxygen during thermal reduction of graphene oxide studied by infrared absorption spectroscopy. *Journal of Physical Chemistry C*, *115*(40), 19761–19781. https://doi.org/10.1021/jp2052618.

Ajala, O. J.; J. O. Tijani; M. T. Bankole and A. S. Abdulkareem. (2022). A critical review on graphene oxide nanostructured material: Properties, Synthesis, characterization and application in water and wastewater treatment. *Environmental Nanotechnology, Monitoring & Management*, *18*, 100673. https://doi.org/10.1016/J.ENMM.2022.100673.

Baker, S. N. and Baker, G. A. (2010). 'Luminescent carbon nanodots: emergent nanolights.', *Angewandte Chemie (International ed. in English)*. Germany, 49(38), pp. 6726–6744. doi: 10.1002/anie.200906623.

Björkman, Å. (1969). 'Thermische Klärschlammbehandlung', *Schweizerische Zeitschrift für Hydrologie*, 31(2), pp. 632–645. doi: 10.1007/BF02543692.

Caņado, L. G.; K. Takai; T. Enoki; M. Endo; Y. A. Kim; H. Mizusaki; A. Jorio; L. N. Coelho; R. Magalhães-Paniago and M. A. Pimenta. (2006). General equation for the determination of the crystallite size la of nanographite by Raman spectroscopy. *Applied Physics Letters*, *88*(16), 1–4. https://doi.org/10.1063/1.2196057.

Cançado, L. G.; A. Jorio; E. H. M. Ferreira; F. Stavale; C. A. Achete; R. B. Capaz; M. V. O. Moutinho; A. Lombardo; T. S. Kulmala and A. C. Ferrari. (2011). Quantifying defects in graphene via Raman spectroscopy at different excitation energies. *Nano Letters*, *11*(8), 3190–3196. https://doi.org/10.1021/nl201432g.

Cançado, L. G.; M. G. Da Silva; E. H. Martins Ferreira; Hof, F., Kampioti, K., Huang, K., Pénicaud, A., Achete, C. A., Capaz, R. B., and Jorio, A. (2017). Disentangling contributions of point and line defects in the Raman spectra of graphene-related materials. *2D Materials*, *4*(2). https://doi.org/10.1088/2053-1583/aa5e77.

Ferrari, A. C. (2007). 'Raman spectroscopy of graphene and graphite: Disorder, electron-phonon coupling, doping and nonadiabatic effects', *Solid State Communications*, 143(1–2), pp. 47–57. doi: 10.1016/j.ssc.2007.03.052.

Ferrari, A. C. and Basko, D. M. (2013). 'Raman spectroscopy as a versatile tool for studying the properties of graphene', *Nature Nanotechnology*, 8(4), pp. 235–246. doi: 10.1038/nnano.2013.46.

Frank, O. and Kalbac, M. (2014). 'Chemical vapor deposition (CVD) growth of graphene films', in *Graphene: Properties, Preparation, Characterisation and Devices*. Second Edi, pp. 27–49. doi: 10.1533/9780857099334.1.27.

Gao, Y., Wang, C., Zhang, J., Jing, Q., Ma, B., Chen, Y., and Zhang, W. (2020). Graphite Recycling from the Spent Lithium-Ion Batteries by Sulfuric Acid Curing-Leaching Combined with High-Temperature Calcination. *ACS Sustainable Chemistry and Engineering*, *8*(25), 9447–9455. https://doi.org/10.1021/acssuschemeng.0c02321

Hou, D., Liu, Q., Wang, X., Quan, Y., Qiao, Z., Yu, L., and Ding, S. (2018). Facile synthesis of graphene via reduction of graphene oxide by artemisinin in ethanol. *Journal of Materiomics*, *4*(3), 256–265. https://doi.org/10.1016/j.jmat.2018.01.002

Htwe, Y. Z. N., Chow, W. S., Suda, Y., Thant, A. A., and Mariatti, M. (2019). Effect of electrolytes and sonication times on the formation of graphene using an electrochemical exfoliation process. *Applied Surface Science*, *469*, 951–961. https://doi.org/10.1016/j.apsusc.2018.11.029

Hu, M.; Z. Yao and X. Wang. (2017). 'Characterization techniques for graphene-based materials in catalysis', *AIMS Materials Science*, 4(3), pp. 755–788. doi: 10.3934/matersci.2017.3.755.

Ilias, S. H., Murshidi, J. A. and Ying, K. K. (2021). 'Effect of electrolyte concentration on the synthesis of graphene by electrochemical exfoliation process', *IOP Conference Series: Materials Science and Engineering*, 1106(1), p. 012013. doi: 10.1088/1757-899x/1106/1/012013.

Jorio, A., Saito, R., Dresselhaus, G., and Dresselhaus, M. S. (2011). Dispersive G′-Band and Higher-Order Processes: The Double Resonance Process. In *Raman Spectroscopy in Graphene Related Systems* (Issue 2, pp. 277–298). https://doi.org/10.1002/9783527632695.ch12

Kurian, M. (2021). 'Recent progress in the chemical reduction of graphene oxide by green reductants–A Mini review', *Carbon Trends*. Elsevier Ltd, 5, pp. 100–120. doi: 10.1016/j.cartre.2021.100120.

Larouche, N. and Stansfield, B. L. (2010). 'Classifying nanostructured carbons using graphitic indices derived from Raman spectra', *Carbon*. Elsevier Ltd, 48(3), pp. 620–629. doi: 10.1016/j.carbon.2009.10.002.

Lee, H., Choi, J. Il, Park, J., Jang, S. S., and Lee, S. W. (2020). Role of anions on electrochemical exfoliation of graphite into graphene in aqueous acids. *Carbon*, *167*, 816–825. https://doi.org/10.1016/j.carbon.2020.06.044.

Lee, H. C., Liu, W. W., Chai, S. P., Mohamed, A. R., Aziz, A., Khe, C. S., Hidayah, N. M. S., and Hashim, U. (2017). Review of the synthesis, transfer, characterization and growth mechanisms of single and multilayer graphene. *RSC Advances*, *7*(26), 15644–15693. https://doi.org/10.1039/C7RA00392G

Lellala, K.; K. Namratha and K. Byrappa. (2016). 'Ultrasonication assisted mild solvothermal synthesis and morphology study of few-layered graphene by colloidal suspensions of pristine graphene oxide', *Microporous and Mesoporous Materials*. Elsevier Ltd, 226, pp. 522–529. doi: 10.1016/j.micromeso.2016.01.036.

Li, D., Yang, Z., Jia, D., Wu, D., Zhu, Q., Liang, B., Wang, S., and Zhou, Y. (2016). Microstructure, oxidation and thermal shock resistance of graphene reinforced SiBCN ceramics. *Ceramics International*, *42*(3), 4429–4444. https://doi.org/10.1016/j.ceramint.2015.11.127

Li, L., Zhang, D., Deng, J., Fang, J., and Gou, Y. (2020). Review—Preparation and Application of Graphene-Based Hybrid Materials through Electrochemical Exfoliation. *Journal of The Electrochemical Society*, *167*(8), 086511. https://doi.org/10.1149/1945-7111/ab933b

Liu, F., Wang, C., Sui, X., Riaz, M. A., Xu, M., Wei, L., and Chen, Y. (2019). Synthesis of graphene materials by electrochemical exfoliation: Recent progress and future potential. *Carbon Energy*, *1*(2), 173–199. https://doi.org/10.1002/cey2.14

Liu, J., Shi, H., Hu, X., Geng, Y., Yang, L., Shao, P., and Luo, X. (2022). Critical strategies for recycling process of graphite from spent lithium-ion batteries: A review. *Science of the Total Environment*, *816*, 151621. https://doi.org/10.1016/j.scitotenv.2021.151621

Liu, L., Qing, M., Wang, Y., and Chen, S. (2015). Defects in Graphene: Generation, Healing, and Their Effects on the Properties of Graphene: A Review. *Journal of Materials Science and Technology*, *31*(6), 599–606. https://doi.org/10.1016/j.jmst.2014.11.019

Liu, Z., Xu, Q., Zhang, C., Sun, Q., Wang, C., Dong, M., Wang, Z., Ohmori, H., Kosinova, M., Goto, T., Tu, R.,

and Zhang, S. (2020). Laser-induced growth of large-area epitaxial graphene with low sheet resistance on 4H-SiC(0001). *Applied Surface Science*, *514*(February), 145938. https://doi.org/10.1016/j.apsusc.2020.145938.

Matthews, M. J.; M. A. Pimenta; G. Dresselhaus; M. S. Dresselhaus and M. Endo. (1999). Origin of dispersive effects of the Raman D band in carbon materials. *Physical Review B - Condensed Matter and Materials Physics*, *59*(10), 6585–6588. https://doi.org/10.1103/physrevb.59.r6585.

Mbayachi, V. B.; E. Ndayiragije; T. Sammani; S. Taj; E. R. Mbuta and khan, A. ullah. (2021). Graphene synthesis, characterization and its applications: A review. *Results in Chemistry*, *3*, 100163. https://doi.org/10.1016/j.rechem.2021.100163.

Melchor-Martínez, E. M.; R. Macias-Garbett; A. Malacara-Becerra; H. M. N. Iqbal; J. E. Sosa-Hernández and R. Parra-Saldívar. (2021). Environmental impact of emerging contaminants from battery waste: A mini review. *Case Studies in Chemical and Environmental Engineering*, *3*(April). https://doi.org/10.1016/j.cscee.2021.100104.

Munuera, J. M.; J. I. Paredes; S. Villar-Rodil; M. Ayán-Varela A. Martínez-Alonso and J. M. D. Tascón. (2016). Electrolytic exfoliation of graphite in water with multifunctional electrolytes: En route towards high quality, oxide-free graphene flakes. *Nanoscale*, *8*(5), 2982–2998. https://doi.org/10.1039/c5nr06882g.

Munuera, J. M.; J. I. Paredes; M. Enterría; A. Pagán; S. Villar-Rodil; M. F. R. Pereira; J. I. Martins; J. L. Figueiredo; J. L. Cenis; A. Martínez-Alonso and J. M. D. Tascón. (2017). Electrochemical Exfoliation of Graphite in Aqueous Sodium Halide Electrolytes toward Low Oxygen Content Graphene for Energy and Environmental Applications. *ACS Applied Materials and Interfaces*, *9*(28), 24085–24099. https://doi.org/10.1021/acsami.7b04802.

Nemanich, R. J. and Solin, S. A. (1979) 'First- and second-order Raman scattering from finite-size crystals of graphite', *Physical Review B*, 20(2), pp. 392–401. doi: 10.1103/PhysRevB.20.392.

Pimenta, M. A.; G. Dresselhaus; M. S. Dresselhaus; L. G. Cançado; A. Jorio and R. Saito. (2007). Studying disorder in graphite-based systems by Raman spectroscopy. *Physical Chemistry Chemical Physics*, *9*(11), 1276–1291. https://doi.org/10.1039/b613962k.

Pollard, A. J.; B. Brennan; H. Stec; B. J. Tyler; M. P. Seah; I. S. Gilmore and D. Roy. (2014). Quantitative characterization of defect size in graphene using Raman spectroscopy. *Applied Physics Letters*, *105*(25). https://doi.org/10.1063/1.4905128.

Razaq, A.; F. Bibi; X. Zheng; R. Papadakis; S. H. M. Jafri and H. Li. (2022). Review on Graphene-, Graphene Oxide-, Reduced Graphene Oxide-Based Flexible Composites: From Fabrication to Applications. *Materials*, *15*(3), 1–17. https://doi.org/10.3390/ma15031012.

Rey, I.; C. Vallejo; G. Santiago; M. Iturrondobeitia and E. Lizundia. (2021). Environmental Impacts of Graphite Recycling from Spent Lithium-Ion Batteries Based on Life Cycle Assessment. *ACS Sustainable Chemistry and Engineering*, *9*(43), 14488–14501. https://doi.org/10.1021/acssuschemeng.1c04938.

Rothermel, S.; M. Evertz; J. Kasnatscheew; X. M. Qi; Grützke; M. Winter and S. Nowak. (2016). Graphite Recycling from Spent Lithium-Ion Batteries. *ChemSusChem*, *9*(24), 3473–3484. https://doi.org/10.1002/cssc.201601062.

Shearer, C. J.; A. D. Slattery; A. J. Stapleton; J. G. Shapter and C. T. Gibson. (2016). Accurate thickness measurement of graphene. *Nanotechnology*, *27*(12), 0. https://doi.org/10.1088/0957-4484/27/12/125704.

Shen, C.; J. E. Calderon; E. Barrios; M. Soliman; A. Khater; A. Jeyaranjan; L. Tetard; A. Gordon; S. Seal; and L. Zhai. (2017). Anisotropic electrical conductivity in polymer derived ceramics induced by graphene aerogels. *Journal of Materials Chemistry C*, *5*(45), 11708–11716. https://doi.org/10.1039/c7tc03846a.

Shinde, D. B.; J. Brenker; C. D. Easton; R. F. Tabor; A. Neild and M. Majumder. (2016). Shear Assisted Electrochemical Exfoliation of Graphite to Graphene. *Langmuir*, *32*(14), 3552–3559. https://doi.org/10.1021/acs.langmuir.5b04209.

Singh, R. (2021). 'Recent Progress in the Electrochemical Exfoliation of Colloidal Graphene: A Review', in *Colloids - Types, Preparation and Applications*. Rijeka: IntechOpen, p. Ch. 2. doi: 10.5772/intechopen.95522.

Sinterhauf, A.; G. A. Traeger; D. Momeni; K. Pierz; H. W. Schumacher and M. Wenderoth.(2021). Unraveling the origin of local variations in the step resistance of epitaxial graphene on SiC: a quantitative scanning tunneling potentiometry study. *Carbon*, *184*, 463–469. https://doi.org/10.1016/j.carbon.2021.08.050.

Toh, S. Y.; K. S. Loh; S. K. Kamarudin and W. R. W. Daud. (2014). Graphene production via electrochemical reduction of graphene oxide: Synthesis and characterisation. *Chemical Engineering Journal*, *251*, 422–434. https://doi.org/10.1016/j.cej.2014.04.004.

Tran, T. X; H. Choi; C. H. Che; J. H. Sul; I. G. Kim; S. M. Lee; J. H. Kim and In, J. Bin. (2018). Laser-Induced Reduction of Graphene Oxide by Intensity-Modulated Line Beam for Supercapacitor Applications [Research-article]. *ACS Applied Materials and Interfaces*, *10*(46), 39777–39784. https://doi.org/10.1021/acsami.8b14678.

Wang, J.; X. Jin; C. Li; W. Wang; H. Wu and S. Guo. (2019). Graphene and graphene derivatives toughening polymers: Toward high toughness and strength. In *Chemical Engineering Journal*. Elsevier B.V. https://doi.org/10.1016/j.cej.2019.03.229.

Wu, J.; Bin; M. L. Lin; X. Cong; H. N. Liu and P. H. Tan. (2018). Raman spectroscopy of graphene-based materials and its applications in related devices. *Chemical Society Reviews*, *47*(5), 1822–1873. https://doi.org/10.1039/c6cs00915h.

Wu, Z. S.; W. Ren; L. Gao; B. Liu; C. Jiang and H. M. Cheng. (2009). Synthesis of high-quality graphene with a pre-determined number of layers. *Carbon*, *47*(2), 493–499. https://doi.org/10.1016/j.carbon.2008.10.031.

Xie, X.; Y. Zhou and K. Huang. (2019). 'Advances in microwave-assisted production of reduced graphene oxide', *Frontiers in Chemistry*, 7(Jun), pp. 1–11. doi: 10.3389/fchem.2019.00355.

Yoo, D.; Y. Park; B. Cheon and M.-H. Park. (2019). Carbon Dots as an Effective Fluorescent Sensing Platform for Metal Ion Detection. *Nanoscale Research Letters*, *14*(272), 1–13. https://doi.org/10.1186/s11671-019-3088-6.

Yoon, G.; D. H. Seo; K. Ku; J. Kim; S. Jeon and K. Kang. (2015). Factors affecting the exfoliation of graphite intercalation compounds for graphene synthesis. *Chemistry of Materials*, *27*(6), 2067–2073. https://doi.org/10.1021/cm504511b.

Yue, W.; Y. Liu; M. Zhao; F. Ye and L. Cheng. (2019). Effect of heat treatment temperature on microstructure and electromagnetic shielding properties of graphene/SiBCN composites. *Journal of Materials Science & Technology*. https://doi.org/10.1016/j.jmst.2019.07.018.